

Multistability of oscillatory thermocapillary convection in a liquid bridge

V. M. Shevtsova, D. E. Melnikov, and J. C. Legros*

MRC, CP-165/62, Université Libre de Bruxelles, 50, Avenue F. D. Roosevelt, B-1050 Brussels, Belgium

(Received 28 April 2003; published 31 December 2003)

A parametric investigation of the onset of chaos in a liquid bridge was numerically carried out for a medium Prandtl number liquid, $Pr = 4$, and unit aspect ratio under zero-gravity conditions. Spatiotemporal patterns of thermocapillary flow were successively studied beginning from the onset of instability up to the appearance of the nonperiodic flow and further on. Well-tested numerical code is used for solving the three-dimensional time-dependent Navier-Stokes equations in cylindrical coordinate system. Two-dimensional steady flow becomes oscillatory with azimuthal wave number $m=2$ as a result of Hopf bifurcation at $Re_1^{cr} = 630$. A second independent solution with wave number $m=3$ was found to appear at Reynolds number $Re_2^{cr} \approx 810$. Two branches of three-dimensional periodic orbits, traveling waves with $m=2$ and $m=3$, coexist for $Re > Re_2^{cr}$. Additional stable branches do not connect them. The different flow organizations reveal different behaviors in the supercritical area. The $m=2$ traveling wave always remains periodic, but the mode $m=3$ starts exhibiting chaotic features at $Re \approx 4200$. The onset of temporal nonperiodicity was shown to be associated with development of broadband noise in spectra and preceded by a quasiperiodicity. The flow stabilizes back to periodic with single frequency when Re exceeds a value $Re \approx 5100$. The window of periodicity exists up to at least $Re = 6000$, the largest investigated value of the Reynolds number.

DOI: 10.1103/PhysRevE.68.066311

PACS number(s): 47.27.-i, 47.35.+i, 05.45.Pq, 47.20.Dr

I. INTRODUCTION

Investigation of convective flows in systems with free interface attracts a lot of attention, specifically due to their relevance to crystal growth processes under microgravity conditions. Temperature gradients along the interface between two immiscible fluids cause variations of surface tension resulting in tangential stresses, which can drive bulk flow motion. The stability of such thermoconvective flows was actively studied in a half-zone model, which corresponds to floating zone (FZ) techniques of a crystal growth. Although the FZ method seems to be superior with respect to the other growth technique due to the absence of contact with crucible, it has not gained an importance for the crystal growth on the earth. The reason for that is the limitation by the hydrostatic pressure, permitting only the growth of crystal of small diameter. This drawback, however, can be overcome under microgravity conditions. In the half-zone model (liquid bridge) a small volume of liquid is held between two coaxial circular disks, which are kept at different temperatures, $\Delta T = T_{hot} - T_{cold}$. As the applied temperature gradient is parallel to the interface, motion from the hot to the cold region appears for any nonzero value of ΔT . When the temperature difference between the disks exceeds the critical value, $\Delta T > \Delta T_{cr}$, unique for a given set of parameters, the flow is three dimensional and/or unsteady. Generally, two hydrothermal waves propagating in opposite directions bifurcate from two-dimensional (2D) state at the critical point. They result in standing (SW) or traveling (TW) wave depending on the ratio of their amplitudes. Understanding the evolution of the thermocapillary flows is valuable for material processing in space. The transition from the steady to

oscillatory flow is well comprehended due to the numerical modeling (see for example Wanschura *et al.* [1], Leypoldt *et al.* [2], Lappa *et al.* [3]). These results are supported by the experimental studies, see recent review by Schatz and Neitzel [4].

An increasing number of experimental studies indicates that convection in melt should be turbulent [5]. Nevertheless, because of great complexity of the turbulent flows, all numerical simulations of transport processes were performed assuming laminar flow in the liquid phase. Apart from that, from the more physical side, the hydrodynamics effects in the half-zone model are of basic interest for the dynamics occurring in the system, as it is an excellent example of a dissipative dynamical system. Therefore, the present study is aimed at investigating time-dependent convective flows in the strongly supercritical regimes. The consideration of a liquid bridge from the point of nonlinear physics has been done only experimentally under terrestrial conditions. In one of the first publications in such trend Petrov *et al.* [6] have considered liquid bridges as a nonlinear dynamical system to control an isolated unstable state far away from the critical point for Prandtl number $Pr = 35$.

The transition from steady flow to chaos has been carefully traced in experiments by Ueno *et al.* [7] for silicone oils of 1, 2, and 5 cSt. The flow was visualized simultaneously by two video cameras and time-dependent temperature was recorded by a thermocouple placed slightly inside of the bridge at midheight. They observed numerous bifurcations of the flow on the way to chaos: 2D steady \rightarrow SW(1) \rightarrow TW(1) \rightarrow transition \rightarrow SW(2) \rightarrow TW(2) \rightarrow chaos \rightarrow turbulence. Each of the regimes has been identified through the observation of the suspended particle motion, the surface temperature variation, its Fourier spectrum, and trajectories in phase plane. The evaluations of the correlation dimension and the maximum Lyapunov exponent have also been done for the different flow states.

*Electronic address: vshev@ulb.ac.be; URL: <http://www.ulb.ac.be/polytech/mrc>

For examination of spatiotemporal behavior of the liquids from laminar flow state up to the onset of chaotic motion, Frank and Schwabe [8] have used another approach. In addition to the optical observations (views from above and from the front), up to 15 thermocouples could be placed around one-half of the free surface without touching it. It allowed them to recognize different spatial reasons for quasiperiodic and period-doubling temporal behavior and identify various spatiotemporal chaotic structures. For the liquids with $Pr=7,49,65$ they observed such phenomena as splitting of subharmonics in the Fourier spectrum, locking of quasiperiodic modes, the presence of only odd harmonics, frequency skips.

Although, the mentioned above experiments [7,8] have been done in tiny liquid bridges, the influence of buoyancy force on the nonlinear behavior is not negligible. The present results are targeting on the study of the nonlinear characteristics of the flow under zero-gravity conditions. First of all, the nonlinear system admits regime of bistability. A branch of SW with azimuthal wave number $m=2$ bifurcates from the basic branch of axisymmetric steady state; this branch remains stable in the considered range of parameters. A second stable branch with azimuthal wave number $m=3$ appears later and above the threshold of instability reveals other periodic, quasiperiodic, and chaotic attractors. Our latest calculations of the similar problems under gravity conditions demonstrate quite different behavior of the system with respect to zero-gravity case and will be published elsewhere.

To the best of our knowledge, the bifurcation of thermocapillary flow in a liquid bridge in the strongly supercritical regime has not yet been mapped out. The finite size systems with an open interface along which Marangoni force acts have been out of focus. The transition to chaos has been extensively studied for convective flows in several well-defined systems: Rayleigh-Bénard convection or convection in binary mixtures. Different routes to nonperiodic motion have been identified for convective flows in closed systems by Baker and Gollub [9]. Besides the examination of the multistability properties, one of the goals of this paper is to identify numerically the bifurcation route to chaos for the case of pure thermocapillary convection in cylindrical volume.

II. FORMULATION OF THE PROBLEM

A liquid bridge consists of a fluid volume held between two differentially heated horizontal flat concentric disks of radius R , separated by a distance d . The geometry of the problem is shown in Fig. 1. The temperatures T_h and T_c ($T_h > T_c$) are prescribed at the upper and lower solid-liquid interfaces, respectively, yielding a temperature difference $\Delta T = T_h - T_c$. The surface tension and kinematic viscosity are taken as linear functions of temperature,

$$\sigma(T) = \sigma_0(T_c) - (d\sigma/dT)(T - T_c),$$

$$\nu(T) = \nu_0(T_c) + (d\nu/dT)(T - T_c).$$

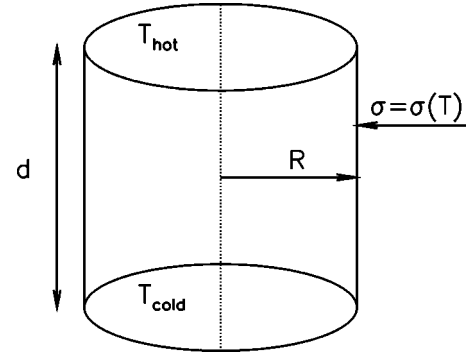


FIG. 1. Geometry of the problem.

The governing Navier-Stokes, energy, and continuity equations are written in nondimensional primitive-variable formulation in cylindrical coordinate system:

$$\frac{\partial \mathbf{V}}{\partial t} + \mathbf{V} \cdot \nabla \mathbf{V} = -\nabla P + 2R_\nu \mathbf{S} \times \nabla (\Theta + z) + [1 + R_\nu (\Theta + z)] \Delta \mathbf{V}, \quad (1)$$

$$\nabla \cdot \mathbf{V} = 0, \quad (2)$$

$$\frac{\partial \Theta}{\partial t} + \mathbf{V} \cdot \nabla \Theta = -V_z + \frac{1}{Pr} \Delta \Theta, \quad (3)$$

where velocity is defined as $\mathbf{V} = (V_r, V_\varphi, V_z)$, $\Theta_0 = (T - T_c)/\Delta T$ is the dimensionless temperature, and Θ is the deviation from the linear temperature profile $\Theta = \Theta_0 - z$, $\mathbf{S} = (1/2)(\partial V_i/\partial x_k + \partial V_k/\partial x_i)$ is the strain rate tensor. One may find the explicit form of these equations in Ref. [10]. The scales for time, velocity, and pressure are $V_{ch} = \nu_0/d$, $t_{ch} = d^2/\nu_0$, and $P_{ch} = \rho_0 V_{ch}^2$. The temperature of the cold disk $T_0 = T_c$ is used as the reference, so $\nu_0 = \nu(T_c)$.

At the rigid walls no slip conditions are used, $\mathbf{V}(r, \varphi, z = 0, t) = 0$, $\mathbf{V}(r, \varphi, z = 1, t) = 0$, and constant temperatures are imposed, $\Theta(r, \varphi, z = 0, t) = 0$, $\Theta(r, \varphi, z = 1, t) = 0$.

For the particular case $V = \pi R^2 d$ in the absence of gravity the liquid volume takes an upright cylindrical shape. Here the limit of asymptotically large mean surface tension, σ_0 , is considered, therefore the free surface shape is not influenced by static or dynamic pressure [11]. On the cylindrical free surface ($r = 1, 0 \leq \varphi \leq 2\pi, 0 \leq z \leq 1$), due to the kinematic condition $V_r = 0$ and the stress balances are

$$2[1 + R_\nu (\Theta + z)] \mathbf{S} \cdot \mathbf{e}_r + \text{Re} \left(\mathbf{e}_z \partial_z + \mathbf{e}_\phi \frac{1}{r} \partial_\phi \right) (\Theta + z) = 0. \quad (4)$$

The free surface is assumed thermally insulated $\partial_r \Theta(r = 1, \varphi, z, t) = 0$. The Reynolds, Prandtl, Marangoni numbers, the relative variation of the viscosity and aspect ratio are defined as

TABLE I. Effect of the grid resolution on the parameters of supercritical flow, $Re \approx 5 Re_{cr}$.

Grid size	Re	Initial symmetry	Final symmetry	Φ	ω_0
[25×16×21]	3000	$m=2$	$m=2$	6.25×10^{-1}	48.58
[25×16×31]	3000	$m=1$	$m=2$	6.32×10^{-1}	48.61
[25×32×31]	3000	$m=6$	$m=2$	6.67×10^{-1}	48.47
[49×16×41]	3000	$m=4$	$m=2$	6.37×10^{-1}	51.50
[25×16×31]	3000	$m=3$	$m=3$	8.23×10^{-1}	54.56
[49×16×41]	3000	$m=3$	$m=3$	8.88×10^{-1}	59.27

$$Re = \frac{\sigma_T \Delta T d}{\rho_0 \nu_0^2}, \quad Pr = \frac{\nu_0}{k}, \quad Ma = Re Pr, \quad R_\nu = \frac{1}{\nu_0} \frac{\partial \nu}{\partial T} \Delta T,$$

$$\Gamma = \frac{d}{R}. \quad (5)$$

Throughout this parametric study the Prandtl number, the variation of viscosity, and the aspect ratio are kept constant, $Pr=4$, $R_\nu=-0.5$, and $\Gamma=1$. Keeping all the parameters of the problem constant, the flow is controlled by the Reynolds number, which is proportional to the temperature difference between the rods.

III. SOLUTION METHOD

The three-dimensional, fully nonlinear governing equations (1)–(4) were solved in a primitive-variable form on a staggered stretched mesh. The velocity field is defined at the points, which are the central nodes of the cell sides. Values of the scalar variables are stored at the centers of basic cells. Central differences for spatial derivatives and forward differences for time derivatives were utilized for discretization of the equations. These equations were integrated over nonoverlapping finite volumes. The computation of the velocity field at each time step was carried out with the projection method (see, e.g., Fletcher [12]). The singularities at the symmetry axis of the cylindrical domain may cause numerical problems. To overcome these difficulties, velocity on the cylinder axis was calculated separately with a special algorithm, developed by the authors. A combination of fast Fourier transform in the azimuthal direction and of an alternative direction implicit method in the others was applied for calculating the Poisson equation for pressure. The detailed description of the numerical code and its validating procedure near the critical Reynolds number (onset of oscillatory 3D flow) can be found in Ref. [10].

As the present results spread to supercritical values of the Reynolds number, the code validation was extended for this region, when $Re \approx 5 Re_{cr}$. The data in Table I present the results obtained on different grids. Comparison was done for the net azimuthal flow Φ , see definition in Eq. (7), and for the fundamental frequency of oscillations when $Re=3000$. In the case of a final symmetry $m=2$ the results from four different meshes have been compared, where the numbers indicate the amount of the points in the radial, azimuthal, and axial directions, respectively. The variation of the azimuthal flow and the frequency for this highly supercritical Reynolds

number on different grids is about 6%. Optimizing both the quality of the results and time consumption, the basic calculations have been done on the intermediate grid [25×16×31] with smaller space intervals near the hot and, especially, near the cold corner. The relatively low dispersion between the results on the chosen grid and the more fine ones allows us to conclude that the flow and stability features are well resolved. As the present system allows coexistence of two different modes, the convergence is done for both of them. The results of the test for convergence on grid for the flow with $m=3$ symmetry are similar to those for $m=2$, see the last two lines in Table I. Agreement of behavior of the integral and spectral characteristics for the two different grids was a good validation of the code. An additional resolution study concerning inheriting the symmetry will be given in the following section when $Re \approx 10 Re_{cr}$.

For integrating the governing equations at a supercritical Reynolds number, a solution for the previously investigated Re was taken as initial guess. The temperature oscillations were recorded at four azimuthally equidistant points inside the liquid bridge at $r=0.9$ and $z=0.5$. To identify unambiguously the 3D time-dependent flow structure, its axisymmetric component is subtracted from the resulting flow field and the remaining disturbance flow is analyzed. The azimuthal wave number of the periodic oscillatory flow m corresponds to the temperature field structure: it is organized in such a manner, that after the axisymmetric component is subtracted there are m hot and m cold spots observed in a transversal section and on the free surface, see below Figs. 3 and 4.

IV. DESCRIPTION OF RESULTS

A. Multistability of the oscillatory flow

The traveling wave with azimuthal wave number $m=2$ bifurcates from the axisymmetric steady state at $Re_1^{cr}=630$. The 3D oscillatory flow is a result of a supercritical Hopf bifurcation and the periodic orbit represents the unique stable solution near the onset of the instability. Beyond the first critical point $Re \geq Re_2^{cr}=810$, the system admits the coexistence of two stable oscillatory solutions with two different wave numbers $m=2$ and $m=3$. One should remember that these two solutions do not represent the different modes of the linear problem; on the contrary, they are both the results of the solution of the full nonlinear problem, Eqs. (1)–(3). For $Re > Re_2^{cr}$ transitions between the two stable orbits with $m=2$ and $m=3$ have never been observed. The final solution depends on the initially chosen wave-number guess.

Near the threshold of instability the liquid bridge system exhibits only one solution with self-sustained oscillations. Going further to the supercritical area the flow organization

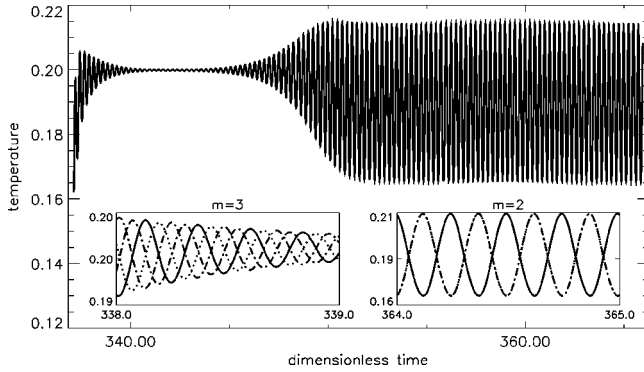


FIG. 2. Ascertainment of stable oscillatory solution with wave number $m=2$. Initial guess is a flow field with a symmetry $m=3$ which is unstable for this set of parameters and finally decays. The temperature profiles correspond to $Re=700$, $Pr=4$, $\Gamma=1$.

with a higher wave number will be excited. For example, Ueno *et al.* [7] and Shevtsova *et al.* [13] have experimentally observed that the wave number switches from $m=1$ to $m=2$ when moving to the far supercritical region of the Reynolds number. In the vicinity of that bifurcating point two different symmetry patterns coexist in a limited range of Reynolds numbers. However, no theoretical results were reported until now, when two solutions with different symmetries coexist over a vast range in Re and not in the form of the mixed mode.

The initial symmetry of the system has different meaning for the real experiment and theory. Concerning the experiments the term “symmetry of perturbations” makes little sense as they have a nonregular stochastic nature. In numerics, the initial symmetry suggests, for example, the form of the perturbations added to the steady two-dimensional solution to initiate the instability. Different initial guesses may execute various modes in calculations. For example, if the initial perturbations introduced into the system are of the form $\sin(m_1\varphi)$, the solution will be described by the same $\sin(m_1\varphi)$ function if this oscillatory solution is stable. Otherwise, after some time it will modify from the initially taken azimuthal wave number m_1 to another solution with a different m_2 which is stable for considered set of parameters. Thus, despite the symmetry of perturbations the system must arrive at a solution in the form of waves with m_2 wave number.

Indeed, for our particular system in the region of the Reynolds numbers $630 < Re < 810$ only the oscillatory flow $m_1=2$ is stable. To prove it, the calculations have been done for $Re=700$ choosing the initial guess with another symmetry $m_2=3$. Results shown in Fig. 2 demonstrate that after decaying the mode $m=3$, the stable solution with $m=2$ wave number is established. Two insertions in Fig. 2 show the data in a smaller time scale at four equidistant points, $\Delta\varphi = \pi/2$, which are located at the same radial and axial positions. The two solutions with different symmetries can be identified according to the phase shift between the signals.

The influence of initial guess symmetry on the final symmetry of stable solution has been carefully studied for the far-supercritical Reynolds numbers $Re=3000, 4500, 6000$. Analysis of the results obtained allows us to propose a kind

TABLE II. Study of the final flow symmetry on different grids, $Re \approx 10 Re_1^{cr}$.

Grid size	Re	Initial symmetry	Final symmetry
$[25 \times 16 \times 31]$	6000	$m=2$	$m=2$
$[25 \times 32 \times 31]$	6000	$m=6$	$m=2$
$[49 \times 16 \times 41]$	6000	$m=1$	$m=2$
$[25 \times 16 \times 31]$	6000	$m=3$	$m=3$
$[25 \times 32 \times 31]$	6000	$m=5$	$m=3$

of a rule of inheriting the parity of initial symmetry for $Re > 810$; namely, taking an initial guess with $m=1, 2, 4, 6, \dots$, symmetries, after some transient time the system will arrive to $m=2$ solution. Otherwise, all the odd basic symmetries (except $m=1$) give final state of the system with $m=3$. For the largest Reynolds number, $Re=6000$, this test has been successfully performed on three different grids; the information is given in Table II. Note that even wave-number basic symmetries take more computational time to pass the transient period and attain final stable solution than the odd ones.

The snapshots of the temperature disturbances field in a horizontal transversal section ($z=0.5$) and on the free surface are shown in Fig. 3 when $Re=1500$ for flow patterns of different symmetries. The position of $\varphi=0$ corresponds to the horizontal line passing through the circle center and the positive direction for φ is counterclockwise direction. The temperature field with two hot (bright) and two cold (dark) spots in Fig. 3(a) represents TW with a mode $m=2$, and the snapshots with three hot and three cold spots in Fig. 3(b) confirm the existence of a periodic solution with $m=3$. Note that in both cases the waves propagate practically azimuthally, the angles between the spots and z axis on the free surface in Fig. 3 are close to zero. To understand the bulk

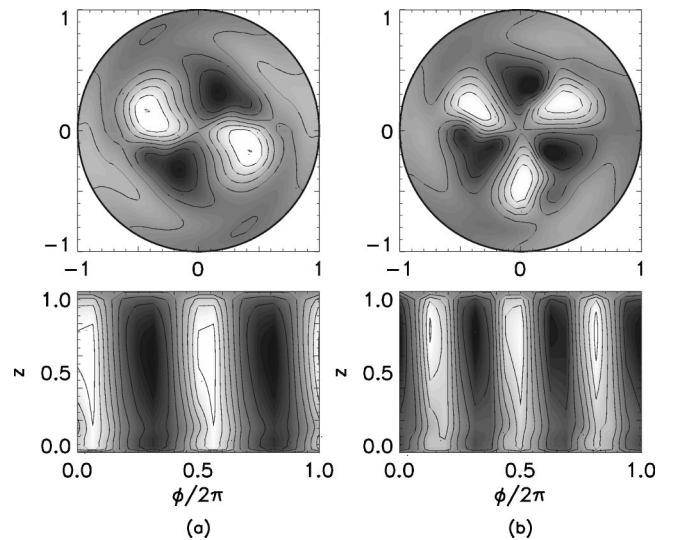


FIG. 3. Temperature disturbance fields in a $z=0.5$ horizontal cross section (upper part) and on the free surface (lower part) for $Pr=4$, $Re=1500$, $\Gamma=1$, $R_v=-0.5$. (a) $m=2$ and (b) $m=3$ solutions. The axisymmetric part is subtracted from the total temperature distribution.

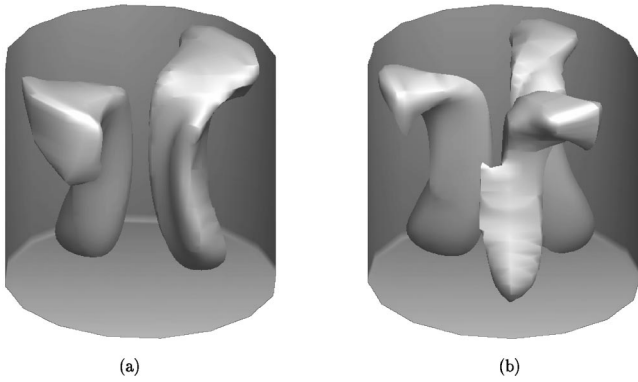


FIG. 4. Surfaces of constant temperature disturbance fields for different symmetry patterns in three-dimensional representation for $Pr=4$, $Re=1500$, $\Gamma=1$, $R_\nu=-0.5$. (a) $m=2$ and (b) $m=3$ solutions.

structure of the temperature disturbances, the three-dimensional images of surfaces of the constant temperature distributions are shown in Fig. 4 for the same set of parameters. Again, the axisymmetric part is subtracted from the total temperature field. For both solutions the snapshots display the surfaces of the same disturbance temperature, $\bar{\Theta} = \Theta_{min} + 0.65(\Theta_{max} - \Theta_{min})$, where Θ_{max} and Θ_{min} are the maximal and minimal values of Θ in the bulk. In both patterns presented in Fig. 4, the surfaces are slightly twisted which is a reflection of one of the features of the traveling waves (in case of standing waves they would be vertically straight).

Note that in the case of $m=2$ solution the two spots and surfaces of constant temperature disturbances have the azimuthal symmetry. For the $m=3$ solution, the symmetry in azimuthal direction is broken even at the moderate Reynolds number, when the flow is still periodic. It is clearly seen in Fig. 4(b) that the closest surface has a kind of spike, while the two others, they do not.

B. Spatiotemporal properties of TW $m=2$

At Reynolds numbers close to the threshold of instability, $Re_1^{cr} = 630$, traveling wave with azimuthal wave number $m=2$ represents the only stable solution. The smooth extension of the limit cycle in phase space near the critical point indicates the supercritical Hopf bifurcation. The growing oscillations saturate on a nearby limit cycle. The radius of the limit cycle is proportional to the saturated amplitude of the oscillations. Staying on the $m=2$ solution, the calculations have never led to chaos. There are no signs indicating additional bifurcations of the system, such as frequency skip, period doubling, or quasiperiodicity. Only one fundamental frequency and its harmonics always present in spectra.

Fourier analyses of the temperature time signals have been done for all investigated Reynolds numbers. Results of the Fourier analysis are summarized in Fig. 5, where the main frequency and its two harmonics are shown. To display the highest harmonics, the square root of the amplitudes is drawn. The evolution of the temporal power spectrum with increase of the Reynolds number demonstrates the smooth

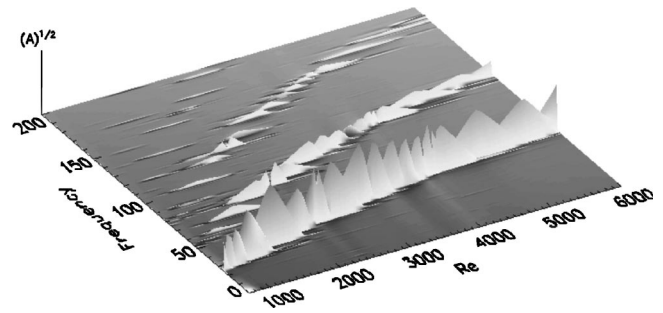


FIG. 5. Evolution of temporal power spectrum with increase of the Reynolds number for the $m=2$ solution. Square root of amplitude is shown. The spectra always have one fundamental frequency and harmonics. No broadband noise is generated.

development of the oscillatory flow. The main frequency retains the leading position in the spectra. The first and second harmonics are clearly visible throughout the investigated region. The maxima of the amplitudes for the different harmonics are dispersed over some region of Reynolds numbers. The amplitude of the main frequency $A_0 = A(\omega_0)$ has a maximum at $Re \approx 2000$, the first and second harmonics achieve maxima at $Re \approx 3000$ and $Re \approx 2500$, respectively.

Ratios of the amplitudes of the harmonics to the amplitude of the main frequency in the appropriate powers as a function of Re are shown in Fig. 6(a), because they are produced by nonlinearity. The generation of higher harmonics is an imminent consequence on the nonlinearity, and their growth is not necessarily related to bifurcations. The functions in Fig. 6(a) do not reveal any jumps, which might be a sign that there is no bifurcation for the $m=2$ solution. The first weak transition in the system occurs at $Re \approx 1000$. As it follows from Fig. 6(a) in the vicinity of this point the amplitude A_1 starts growing up. It never dominates A_0 but results in transformation of the signals.

To characterize the state of the system (attractor), one should calculate some invariant of the motion dynamics.

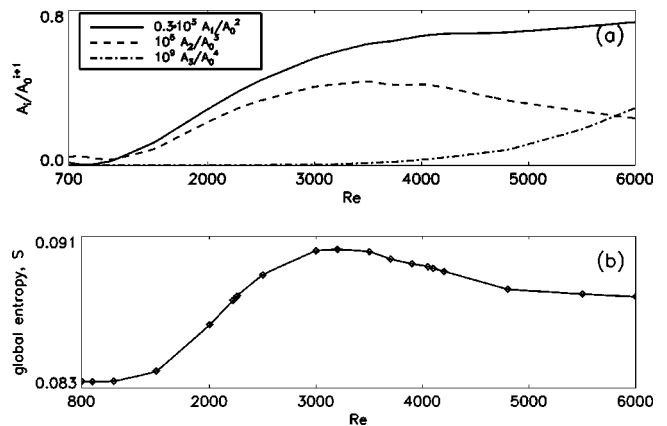


FIG. 6. Ratios of the amplitudes of harmonics to the fundamental frequency in the appropriate powers (a) and global entropy (b), Eq. (6), as functions of the Reynolds number for $m=2$ traveling wave. $A_i, i=1,2$ etc., means the amplitude of the i th harmonic, A_0 is the fundamental frequency. The rhombs correspond to the calculated points, and the solid line is the result of spline interpolation.

Here the entropy S is chosen for describing the spatiotemporal behavior of the system. The entropy is an integral quantity, taking its birth in thermodynamics and statistics, and is a criterion of how well the system is ordered and structured. To see the contribution of the dynamically important modes, the zero mode, representing the spatiotemporal average value of the signal, was excluded from the calculation of the global entropy as it contains a large percentage of the total energy of the system. Conventionally, the global entropy is defined as follows:

$$S(\text{Re}) = -\frac{1}{\ln(N-1)} \sum_{n=1}^N p_n \ln p_n, \quad p_n = \frac{a_n^2}{\sum_{j=1}^N a_j^2}, \quad (6)$$

where a_j are eigenvalues of the spectrum, and the frequency spectra are calculated using the fast Fourier transform from the time series of $N=4096$ points, $\Theta(t) = \sum_{n=0}^N a_n \exp[i(\omega_n t + \varphi_n)]$. To designate the amplitude of the fundamental frequency ω_0 and its harmonics, the following is assumed: $a(k \omega_0) = A_{k-1}$.

The entropy, providing a sign of the relative complexity of the signals, is sensitive to each change of the dynamics. S tends to grow when modulation or bifurcation occurs in the system. Figure 6(b) shows how the entropy follows any change of spatiotemporal organization. In agreement with the previous analysis, its behavior does not reveal any abrupt transition in the system. Comparing Figs. 6(a) and 6(b), one can see that behaviors of the entropy and of the ratio A_1/A_0^2 (solid line) are rather well synchronized near the threshold. Indeed, the entropy starts noticeably to grow at $\text{Re} \approx 1000$ when the first harmonic with distinguishable amplitude appears in the system. The maximal slope $dS/d\text{Re}$ is attained when the higher harmonics start to grow. The entropy increase is associated with a more uniform distribution of energy among the superior eigenvalues. The entropy approaches to a maximum at $\text{Re} \approx 3500$, when the ratio A_2/A_0^3 is close to maximum. It occurs due to overall income of the highest eigenvalues. After some transient time passed, S decrease means that the system approaches a local state of equilibrium.

Equation (6) has been normalized with the Shannon entropy for a completely random process. Such normalization means that S will converge to the highest possible unity value, $S \rightarrow 1$, as the data approach true randomness (white noise). For the considered type of thermocapillary flow, $m=2$, the peak value $S=0.09$ indicates that a quite ordered flow field oscillates in the liquid bridge. The total variation of the entropy is about 8%, although the governing parameters were changed in a large range, $0 < \varepsilon < 8.25$. Here

$$\varepsilon = (\text{Re} - \text{Re}^{cr}) / \text{Re}^{cr}$$

is the distance from the critical point. The situation, when the entropy stays practically constant with Re , physically means that the energy is spread over a few eigenvalues (harmonics). This is coherent with the information coming from Figs. 5 and 6.

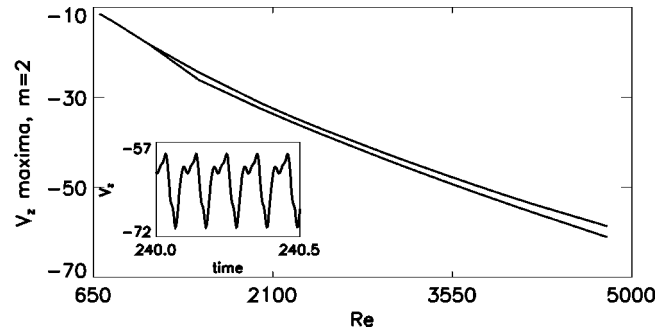


FIG. 7. The evolution of the maxima of axial velocity signals as the Reynolds number increases for $m=2$ oscillatory solution. One-maximum oscillations undergo transition to two-maxima ones at $\text{Re} \approx 1000$.

Note that the same plots made for the axial velocity are identical to the temperature ones presented in Fig. 6(a). The difference is that at $\text{Re} \approx 1000$ the oscillations of axial velocity switched from one-maximum to two-maxima ones (Fig. 7). This type of oscillations, $V_z(t)$, are exposed inside the insertion in Fig. 7. Moving on to higher values of the Reynolds number, difference between the maxima of axial velocity remains constant with good accuracy. It is found that the phase shift between the first harmonic and the fundamental frequency is responsible for the splitting of the maximum, e.g., $V(t) = \sum_i V_i \cos(\omega_i t + \alpha_i)$, where $\alpha_i \neq \alpha_j$, if $i \neq j$. Unlike the velocity behavior, the temperature oscillations contain one maxima throughout the investigated range of the Reynolds number. In this case the phase shift is equal to zero and, respectively, no second maximum is observed.

Despite the fact that the $m=2$ motion is strictly time periodic up to $\text{Re}=6000$ the three different regimes have been determined. Analyzing carefully the behavior of different harmonics and their ratios it appears that existence of these regimes can be disclosed by dependence $\ln(A_1)$ versus $\ln(A_0)$ with the increase of Reynolds number, see Fig. 8. For a better understanding the Roman figures mark the different regimes and a few Reynolds numbers are written along the curve. Comparison of the flow patterns and temperature fields does not exhibit distinctive features of the various regimes, but they can be described through nonlinear characteristics.

(1) Near-threshold weakly nonlinear oscillations, $630 \leq \text{Re} < 1000$, where the limit cycle is *the circle*. The peak-splitting phenomenon of the axial velocity oscillations, see

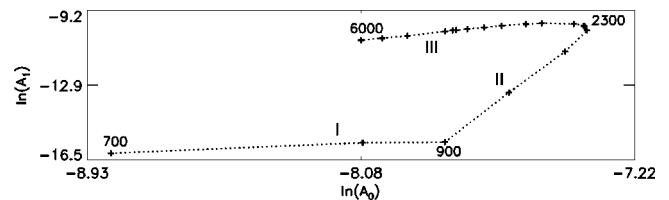


FIG. 8. The dependence of the logarithms of the first harmonic amplitude A_1 on the amplitude of main frequency A_0 when the Reynolds number increases from $\text{Re}=700$ up to $\text{Re}=6000$. Despite the strictly time-periodic oscillations of Θ and V the three different regimes are seen for the $m=2$ solution.

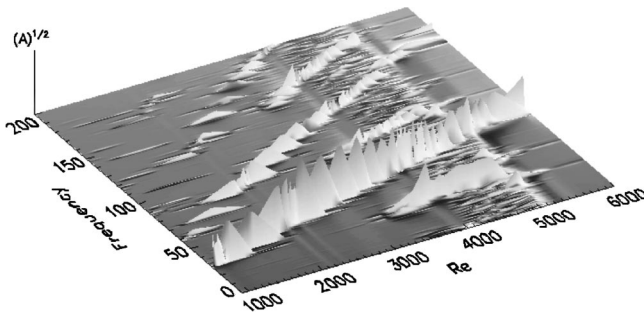


FIG. 9. Evolution of temporal power spectrum with increase of the Reynolds number for the $m=3$ solution. Square root of amplitude is drawn. The second incommensurate frequency exists for $3300 < \text{Re} < 5300$. The broadband noise is developed at $4200 < \text{Re} < 5000$ causing the aperiodic oscillations.

Fig. 7, starts at the end of this regime.

(2) Strongly nonlinear oscillations where the first harmonic A_1 rapidly grows, $1000 < \text{Re} < 2000$, and the shape of limit cycle transforms to a heartlike shape. At the end of this regime the entropy slope $dS/d\text{Re}$ has maximum.

(3) Nonlinear oscillations where the harmonic A_1 is almost independent of the main frequency A_0 , and the former decreases much slower than the latter, $2300 < \text{Re} < 6000$. The dependence $\ln(A_3)$ on $\ln(A_0)$ demonstrates growth of A_3 at this regime (not shown by plot). The shape of the periodic time signal $\Theta(t)$ slightly deviates from sinusoidal, which causes a further transformation of the limit cycle.

C. Spatiotemporal properties of TW $m=3$

Here we shall discuss the results obtained at values of the Reynolds number far beyond Re_2^{cr} . Again, the Fourier analysis of the temperature time signals has been done for all investigated Reynolds numbers. Results of the Fourier analysis are summarized in Fig. 9. Evolution of the temporal power spectrum with increase of the Reynolds number for the $m=3$ solution is completely different from that for the $m=2$ solutions (see Fig. 5). The solution with $m=3$ wave number admits the presence of a rather strong first harmonic with double frequency $2\omega_0$ in the spectrum just near the threshold of instability. The higher harmonics appear in the spectrum moving above the second critical point $\text{Re} = \text{Re}_2^{cr}$.

Until $\text{Re} = 3300$ the dynamic of the flow demonstrates smooth behavior. For each particular Re the time signals of temperature $\Theta(t)$ and velocities $V(t)$ are periodic with a nonmodulated amplitude. The temperature time dependence

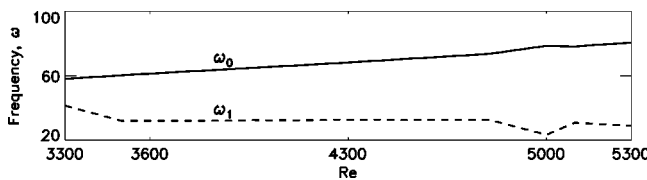


FIG. 10. Main frequencies vs the Reynolds number for the $m=3$ solution. The frequency ω_1 exists only in quasiperiodic and aperiodic phases and slightly beyond the onset of the second periodic dynamics ($3300 \leq \text{Re} \leq 5300$).

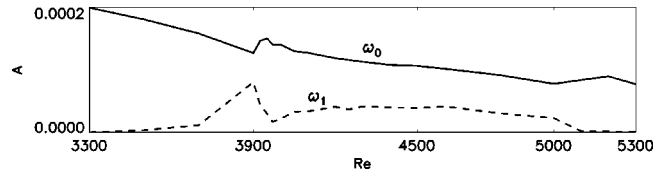


FIG. 11. Amplitudes of the main frequencies (fundamental and the subfrequency) in spectrum for the $m=3$ solution as a function of the Reynolds number.

contains one maxima per period. At $\text{Re} \approx 3300$ the periodic solution with one frequency gives up its stability and an independent frequency ω_1 appears in the spectrum (it is less than the fundamental one, but it is not really a subharmonic). The modulation of time signals $V(t)$ and $\Theta(t)$ is observed from the birth of the frequency ω_1 . The evolution of both frequencies with the Reynolds number and their amplitudes are shown in Figs. 10 and 11. The fundamental frequency ω_0 is almost a linear function of the Reynolds number. At the point $\text{Re} \approx 3300$, where the independent frequency ω_1 has a noticeable amplitude, it has a value of $\omega_1 \approx 30.21$ and is slightly larger than $0.5\omega_0$. As ω_1 remains almost constant, the ratio ω_1/ω_0 decreases with increasing the Reynolds number, and hence at least sometimes their ratio becomes irrational. One can speak about excitation of the two incommensurate frequencies. As a result, in the vicinity of such bifurcations, the flow becomes quasiperiodic. For example, it happens at $\text{Re} \approx 3500$. The representative return map of the oscillations of the axial velocity, proving the realization of the quasiperiodicity one may find in Fig. 12. These return maps (peak-to-peak) maps of axial velocity demonstrate the different regimes of the flow organization. The return map is made in the following way: moving along the records of the

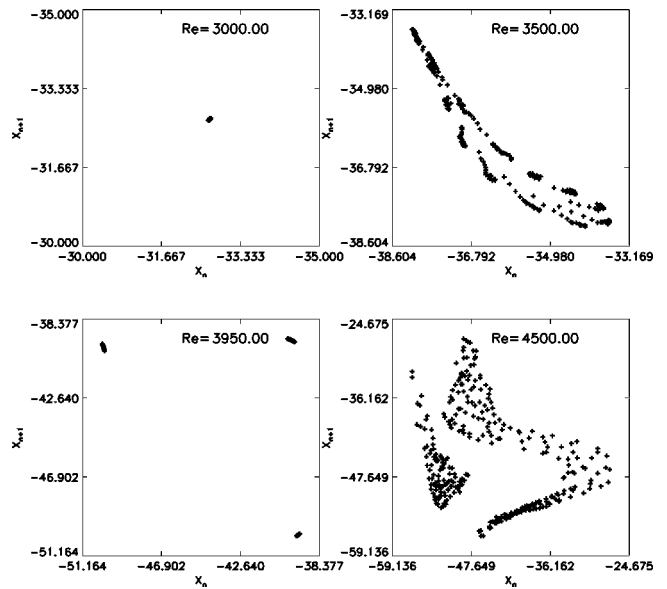


FIG. 12. Return maps of axial velocity for different Reynolds numbers for $m=3$ solution. $\text{Re} = 3000$ —periodic one-frequency oscillations; $\text{Re} = 3500$ —two incommensurate frequency quasiperiodic oscillations; $\text{Re} = 3950$ —period doubling; $\text{Re} = 4500$ —aperiodic oscillations.

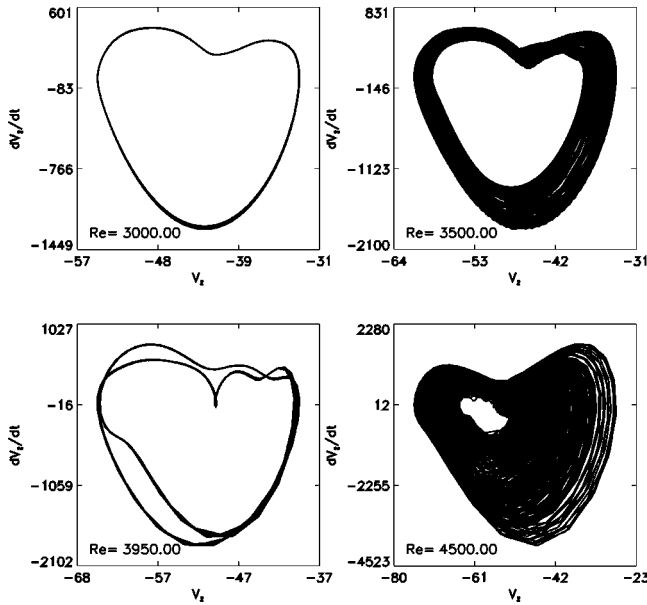


FIG. 13. Phase planes of axial velocity for different Reynolds numbers, $m=3$ solution. $Re=3000$ —periodic one-frequency oscillations; $Re=3500$ —two incommensurate frequency quasiperiodic oscillations; $Re=3950$ —period doubling; $Re=4500$ —aperiodic oscillations.

time signal of axial velocity $V_z(t)$ with a constant time step we search the local maxima. The function X_{n+1} is an amplitude of $(n+1)$ th maximum versus the amplitude X_n of the previous n th maximum.

The ratio ω_1/ω_0 continuously diminishes and never has a plateau, consequently, no phase locking is noticed. As no locking has been observed during the range of Re , where ω_1 exists, one may suggest that the nonlinear interactions between the two oscillations are weak.

The following bifurcation takes place at $Re \approx 3950$. Near this point the frequency ω_1 is slightly larger than half of the fundamental frequency and the latter goes on growing. Inevitably, a period doubling takes place when $\omega_0/\omega_1=2$. The image of this motion in space is T^2 Torus, and the phase plane in Fig. 13 indicates existing of the period-doubling state. It manifests itself in the form of additional loop in the phase plane (Fig. 13) and the return map consists of three points (Fig. 12). The phase planes of axial velocity shown in Fig. 13 correspond to the same setting of the Reynolds numbers as in Fig. 12. The phase plane for the periodic regime, $Re=3000$, represents a close curve but not a perfect circle, as the system is far above from the critical point, $\varepsilon=3.9$.

The typical temperature signal for this range of prechaotic Reynolds numbers, $Re=4000$, and its power spectrum are shown in Fig. 14. Numerous harmonics of comparable power already exist in the spectrum along with the strong long-wave modulation of the temperature time dependence. As the Reynolds number is increased further, the sharp spectral peaks are wiped out by a continuous amplification of dynamical noise (Figs. 14 and 15). The peaks become more numerous and the gaps between them become shallower. It results in a pattern when nonregular oscillatory motion is established. Actually, it is not easy to prove rigorously that a

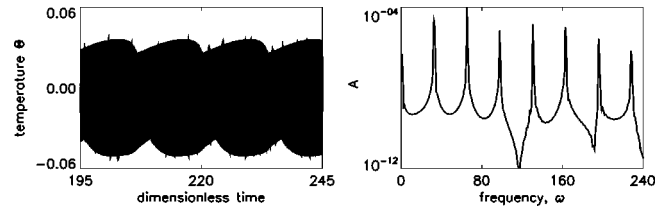


FIG. 14. Temperature record and its power spectrum for $m=3$ solution in the quasiperiodic regime, $Re=4000$. $\omega_0=65.19$, $\omega_1=32.21$.

strange attractor is chaotic. According to our calculations the $m=3$ solution manifests chaotic behavior beginning from $Re \approx 4200$. The strip across the plot in Fig. 9 points out a widespread and featureless distribution of the maxima in the region $4200 \leq Re \leq 5100$. This area looks as a locally “wrinkled tissue.” The weak broadband noise does not conceal the two discrete frequencies but its presence leads to the onset of absolutely continuous spectral background. The presence of noise “washes out” the fine structure of the attractors.

The temporal power spectrum of the temperature is shown in Fig. 15 for $Re=4500$, when aperiodic regime is progressing. Two characteristic frequencies $\omega_0=70.56$ and $\omega_1=32.36$ dominate in the nonperiodic state. Actually, in the power spectrum there is second peak, close to the subfrequency, of more or less the same order of value, see Figs. 9 and 15. This peak really appears to be linear combination $\omega_0 - \omega_1$ within the estimated standard error σ and it may be identified at $3300 < Re < 5100$.

The variation of ω_0 and ω_1 with Re , shown in Fig. 10, illustrates that in the vicinity of the point $Re \approx 5000$ both frequencies have a kind of jump: ω_0 steps up and ω_1 steps down. Shortly after the jump at $Re \approx 5100$ the amplitude of the frequency ω_1 drastically decreases and it completely disappears at $Re \approx 5300$ (see Fig. 11). Along with vanishing the frequency ω_1 nonperiodic flow is stabilized back to periodic at $Re \approx 5100$, and remains periodic until the maximal investigated Reynolds number 6000.

Ratios of the amplitudes of the harmonics to the amplitude of the main frequency in the appropriate powers are drawn in Fig. 16(a) as functions of Re . In accordance with nonlinear theory the ratios of the amplitudes are almost constant near the onset of oscillations. The perfect bifurcation is typically connected with the violation of certain symmetry. Numerous jumps of the functions in Fig. 16(a) in the region $3300 < Re < 5300$ indicate the changes of the flow state and various bifurcations occurring in the system. For example, at

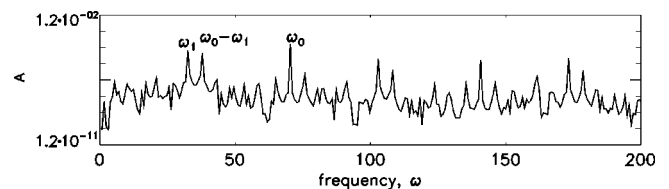


FIG. 15. Temperature temporal power spectrum for $m=3$ solution in the aperiodic regime, $Re=4500$. Two characteristic frequencies $\omega_0=70.56$ and $\omega_1=32.36$.

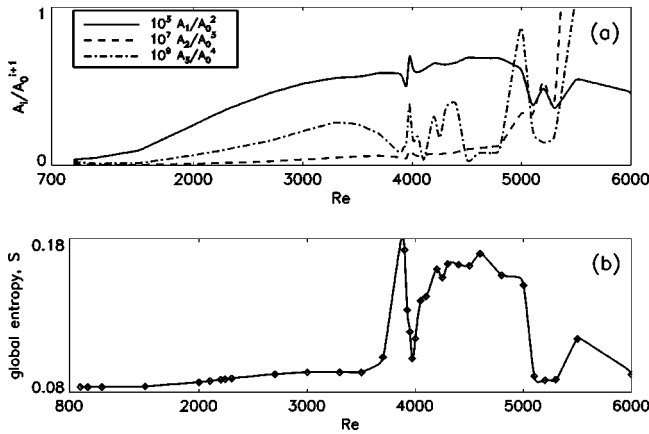


FIG. 16. Ratios of the amplitudes of harmonics to the fundamental frequency in the appropriate powers (a) and global entropy (b), Eq. (6), as functions of the Reynolds number for $m=3$ traveling wave. $A_i, i=1,2, \dots$, means the amplitude of the i th harmonic, A_0 is the fundamental frequency. The rhombs correspond to the calculated points, and the solid line is the result of spline interpolation.

the period-doubling bifurcation $Re \approx 3950$, all curves have a twist. At the beginning of the chaos, $Re \approx 4200$, the ratios A_1/A_0^2 and A_3/A_0^4 have distinguishable local maxima. In the transient regime, aperiodicity \rightarrow periodicity ($5100 \leq Re \leq 5300$), the behavior of the ratios of higher harmonics is very complex. Moreover, at $Re \approx 5200$ the amplitude of the second harmonic, $A(3\omega_0)$, overtakes the amplitude of the first harmonic, $A(2\omega_0)$. Possibly, the second harmonic takes energy from the weak noise in the spectrum and stabilizes the flow. Actually, the interruption of chaotic behavior starts at $Re \approx 5100$ and the signal power spectra become clear, without any noticeable broadband noise and secondary frequencies, see also Fig. 9.

The entropy evolution, see definition in Eq. 6, for the $m=3$ traveling wave is shown in Fig. 16(b). Its behavior reflects the dynamic transitions in the system. Indeed, the entropy slowly augments with appearance of the harmonics in the system when $Re \geq 1500$. It passes smoothly through the quasiperiodic bifurcation and sharply grows up and diminishes in the vicinity of the period-doubling state, $Re \approx 3950$. In the chaotic area, $Re \geq 4200$, when a lot of the harmonics are excited, the entropy again increases. This might be caused by either the spectral noise which contains large percentage of the total energy of the system and “feedbacks” the entropy or an incommensurate frequency. Its non-smooth behavior inside the region of aperiodicity indicates the numerous dynamic changes induced by superior harmonics.

At the end of aperiodicity, $Re \approx 5100$, the entropy drops down and holds some minimal value during the transient regime $5100 \leq Re \leq 5300$. This constancy implies that the energy is distributed over a few harmonics. Indeed, looking at Fig. 9, in this narrow region one should find that two frequencies ω_0 and ω_1 and their linear combinations $\omega = N\omega_0 + M\omega_1$ fill the spectrum but there is no broadband noise. The entropy rises up near $Re \approx 5300$ indicating the dynamic

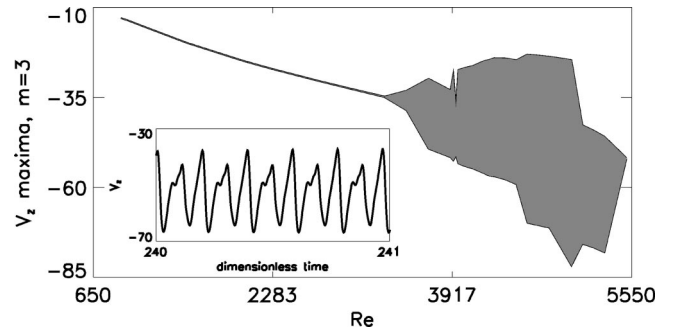


FIG. 17. The evolution of the maxima of axial velocity signals as the Reynolds number increases for $m=3$ oscillatory solution. One-maximum oscillations undergo multimaxima ones at $Re \approx 3300$ and then have only one maxima after $Re \approx 5500$.

change in the system due to the vanishing of the frequency ω_1 . Above $Re \approx 5300$ there is no sign of the presence of ω_1 in the spectrum, only fundamental frequency ω_0 and its harmonics. As a result, the entropy and ratio A_0/A_1^2 diminish.

The behavior of the velocity field is coherent with the temperature evolution, thus oscillations of velocity lose their periodicity at the same ≈ 4200 Reynolds number. Below $Re \approx 3000$ axial velocity performs periodic oscillations with only one maxima and its amplitude is nonmodulated. Shortly before the appearance of the incommensurate frequency the extremum bifurcation gives rise to the splitting of the maxima of the axial velocity, shown in Fig. 17. Peak-splitting phenomenon occurs at $\varepsilon \approx 2.70$ for the $m=3$ pattern while for $m=2$ solution it is observed at $\varepsilon \approx 0.56$ (compare Figs. 7 and 17). A characteristic time signal $V(t)$ with three maxima per period is shown by the insertion in the Fig. 17 for $Re = 3500$. Such kind of time-dependent behavior remains unchanged until $Re \approx 4000$; with further increasing the Reynolds number four or more maxima may encounter. The shaded area is framed by the smallest and largest values of maxima for fixed Re and does not display the amount of them. The splitting of maxima completes at $Re \approx 5500$, soon after the transition of the system from aperiodic to the new periodic regime. The peak-splitting phenomenon is also inherent to the temperature oscillations from the beginning of the quasiperiodic regime.

D. Comparison of the solutions with different wave numbers

Two branches of three-dimensional periodic orbits, traveling waves with $m=2$ and $m=3$, coexist for $Re > Re_2^{c^*}$. The solution with $m=2$ always remains periodic, but the $m=3$ wave number one becomes nonperiodic at $Re^{ch} \approx 4200$. Kudrolli and Gollub [14] reported experimental observation of the coexistence of patterns of different symmetries in forced surface waves (Faraday waves) in the large system limit. These different patterns coexisted only within certain parameter ranges. They obtained that the transition to spatiotemporal chaos depends upon the symmetry of the primary patterns. But, despite the basic symmetry, all patterns finally undergo a transition to chaos. In the present study, we have found different solutions, among which one of them

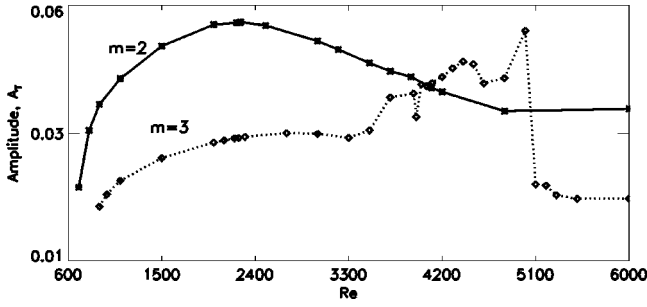


FIG. 18. Amplitudes of temperature oscillations vs the Reynolds number, $A_T = 0.5(\Theta_{max} - \Theta_{min})$. Solid line and asterisks represent $m=2$, while the dashed line with rhombs denotes $m=3$ mode.

does not reveal chaotic features throughout the whole range of the investigated parameters, $\epsilon \leq 8.5$.

The amplitude of the sustained temperature oscillations, defined as $A_T = (\Theta_{max} - \Theta_{min})/2$, is shown in Fig. 18 for both solutions. Solid line with asterisks represents $m=2$ solution, while the dotted line with rhombs corresponds to the $m=3$ solution. The amplitude of the $m=2$ solution increases with the Reynolds number until it reaches a maximum at about $Re = 2300$. No changes in the structure of the thermocapillary flow have been observed near this point. Although, as it was shown in Fig. 8 near this point the nonlinear oscillations undergo transition from II-d to III-d regime, see Fig. 8. With further increase of the Reynolds number the amplitude A_T smoothly diminishes. The temperature amplitude of the $m=3$ solution does not have any pronounced maximum, but its behavior with Re reflects the dynamic transitions in the system. Above the onset of instability the amplitude grows with Re , achieves some saturation value $A_T^* = 0.035$, and remains almost constant when $2300 \leq Re \leq 3000$. At the beginning of the quasiperiodic regime the amplitude starts to grow up. Note that above $Re \approx 3300$ the temperature amplitude is rather strongly modulated. Different types of shorter wave modulations are hidden inside the long-wave modulation, e.g., see Fig. 14. The maximal value of A_T over a longest modulation period is shown in Fig. 18 for the quasiperiodic regime. At the point of period doubling, $Re \approx 3950$, the amplitude jumps down and then goes up. Achieving the aperiodic regime, its (A_T) behavior becomes nonsmooth, being larger than maximal value A_T^* in the periodic regime. The determination of the amplitude of oscillations is more difficult for the aperiodic regime, and it is roughly estimated according to the global extrema on a long time interval. When the system attains the periodic window, $Re \geq 5100$, the amplitude drops down below the initial saturated value A_T^* and continues to decrease.

The evolution of the fundamental frequencies ω_0 with the Reynolds number is shown in Fig. 19. Near the Re_2^{cr} the values of the main frequencies are rather close, e.g., at $Re = 900$ the $m=2$ solution has the frequency $\omega_0 = 27.35$ and $m=3$ has the frequency $\omega_0 = 28.72$. Both solutions demonstrate almost linear dependence of ω_0 upon Re , only the slopes are different. The frequency of the $m=3$ solution grows faster with increase of the Reynolds number. Unlike the evolution of the amplitude, the frequency of the $m=3$

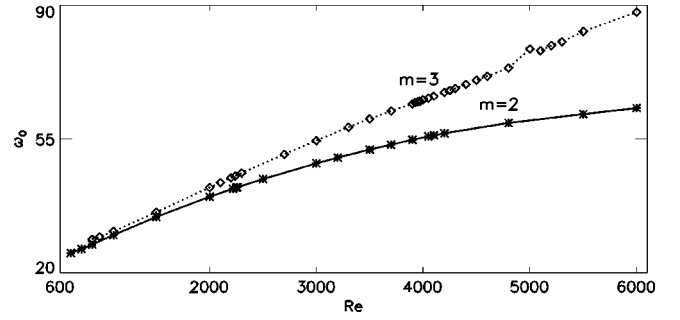


FIG. 19. Dependence of the fundamental frequency upon the Reynolds number. Solid line and asterisks represent $m=2$, while the dashed line with rhombs denote $m=3$ mode.

solution does not trace the dynamic bifurcations in the system. The frequency skip, which often accompanies the dynamic transitions, is not observed here. Possibly, the frequency skip is related with the presence of the gravity force. It was experimentally observed by Frank and Schwabe [8] and by Ueno *et al.* [7] in ground based experiments, and it was numerically determined by Melnikov *et al.* [15] in liquid with $Pr = 18.76$.

The mean azimuthal flow is an important characteristic of the system when 2D thermal convection with periodic boundary conditions becomes unstable. An integral quantity of the flow past bifurcation, the net azimuthal flow, provides information about the nonlinear characteristics of the flow organization. The net azimuthal flow is determined as an integral of the mean azimuthal velocity over the volume:

$$\Phi = \int V_{\varphi,mean}(r,z,t) r dr dz,$$

$$V_{\varphi,mean}(r,z,t) = \frac{1}{2\pi} \int V_{\varphi}(r,z,\varphi,t) d\varphi. \quad (7)$$

Here, $V_{\varphi}(r,z,\varphi,t)$ is the azimuthal velocity. Actually, the resulting mean azimuthal flow includes only nonlinear self-interactions as the contribution of the leading terms is zero owing to the spatial periodicity. Thus nonlinearity of the hydrothermal waves can be described by this net flow. This integral characteristic indicates the intensity of the 3D flow in the case of the traveling wave. The dependence of the mean flow on the Reynolds number is shown in Fig. 20, where solid line and asterisk represent the $m=2$ solution, while rhombs correspond to the $m=3$ flow pattern.

On the net azimuthal flow plot for the $m=3$ solution (Fig. 20) there are two clearly distinct regions related to (a) periodic and to (b) quasiperiodic, aperiodic dynamics. Let us drop the quasiperiodic and aperiodic points off and connect the two regions of periodicity $Re \leq 3300$ and $Re \geq 5100$ using parabolic interpolation technique (dotted line in Fig. 20). Let us nominate this interpolated plot as “regular branch” of the azimuthal net flow. So, in the periodic phase the net azimuthal flow plot and the regular branch coincide. One can clearly see that at $Re = 3300$, the periodic/quasiperiodic bifurcation, the plot starts to deviate from the regular branch (in the quasiperiodic and chaotic region it significantly drops

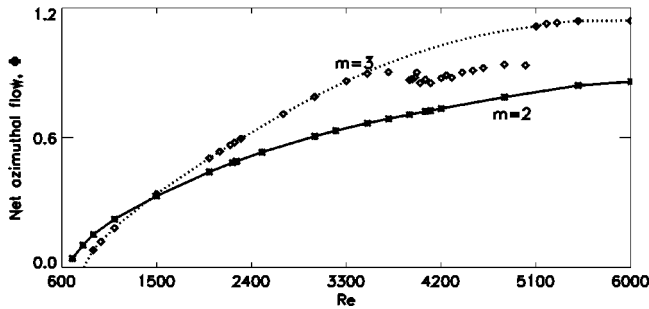


FIG. 20. Net azimuthal flow, defined by Eq. (7), vs the Reynolds number. Solid line and asterisks represent $m=2$ solution, while rhombs denote $m=3$ solution and dotted line corresponds to the regular branch along which the $m=3$ solution is periodic.

off). A quantitative criterion of the deviation from “regularity,” δ_Φ , may be suggested as

$$\delta_\Phi = (\Phi_{reg} - \Phi) / \Phi_{reg}, \tag{8}$$

where Φ is the real calculated value and Φ_{reg} is the value of the net azimuthal flow on the regular branch along which the $m=3$ solution is periodic. The variation of δ_Φ with Re is shown in Table III.

As it follows from Fig. 20 for the quasiperiodic/aperiodic regimes the net azimuthal flow is always below its regular branch Φ_{reg} . Indeed, at the quasiperiodic regime the net flow starts to reduce, see the deviation expressed by δ_Φ in Table III. Within the aperiodic regime, where the disorder is higher, the reduction of the net flow is about of 15–16%. It seems that the energy is transferred from the mean flow into the growing disturbances. In the case of standing wave, due to the symmetry, the net flow is equal to zero, see Ref. [10]. Hence, we may suggest that in the system with periodic boundary conditions, e.g., in a liquid bridge, the standing wave solution will never lead to aperiodicity.

E. Route to aperiodic oscillatory state

The discussion below concerns only the $m=3$ solution. The observed scenario of the onset of aperiodicity in the liquid bridge shows that the present route to chaos may be classified as the quasiperiodicity. The quasiperiodic bifurcation occurs at $Re \approx 3300$ when the second frequency appears (Figs. 9–11).

Analyzing the phase plane portrait of a nonlinear system, one can say that attractor Ω is chaotic if (a) in a state space region the orbits are dense, i.e., they fill the phase space zone of the strange attractor Ω , and (b) the orbits are topologically transitive in Ω , i.e., for any two open sets Ω_1, Ω_2 from Ω there is a time for which any orbit starting at Ω_1 ends at Ω_2 (Wiggins [16]). The first of the criteria can be verified numerically, while the second one is not so easy to be provided

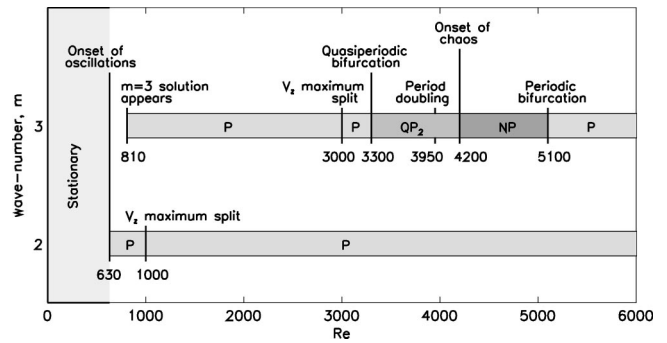


FIG. 21. Schematic graphs of the dynamics of the various stable solutions with the $m=2$ and 3 wave numbers as the Reynolds number increases. $m=2$ traveling wave is always periodic. The solution described by the traveling wave with $m=3$ wave number undergoes aperiodic bifurcation preceded by the quasiperiodic dynamics. The letters inside the bars denote the following: P, periodic; QP_2 , two frequencies quasiperiodic; NP, nonperiodic.

in a simple way. Nevertheless, along with the other observed features of the behavior of the system in this region of the Reynolds number it can be concluded that the orbit for $Re = 4500$ shown in Fig. 13 can be classified as weakly chaotic.

The type of quasiperiodic route, which actually occurs in the system as the control parameter continues increasing, is probably a function of many parameters characterizing the system’s dynamics. The classical scenario could be that a third independent frequency appears, i.e., the attractor becomes a hypertorus. If this attractor is unstable against perturbations, the system dynamics become chaotic. In our case it seems that it is not the distinguishable third frequency, but the broadband spectral noise (a set of incommensurate frequencies), which is responsible for the aperiodicity. Among the known scenarios of the onset of chaos, the concept of Ruelle-Takens (see Refs. [17,18]) is mostly corresponding to the considered system as it takes three bifurcations for the system to get turbulent state. At Re_2^{cr} the attractor takes the form of a periodic orbit, at a larger value of the control parameter the power spectrum has two incommensurate frequencies and the attractor changes to a torus (quasiperiodic phase). Aperiodic regime begins directly from the quasiperiodic one.

The complete dynamic behavior of the system with two symmetry patterns are summarized by the schematic graphs in Fig. 21. The sequence of bifurcations leading to temporal chaos can be identified in the case of the $m=3$ solution. Each bar is labeled by letters P, QP_2 , and NP reading for periodic, two frequencies quasiperiodic, and nonperiodic, respectively. Numbers below the bars denote the values of the Reynolds number at which the marked above events take place.

Note that the spatial Fourier spectra, being discrete for cylindrical geometry, reveal the increasing of the amplitude

TABLE III. Spatial disorganization of the flow δ_Φ , Eq. (6.2), as a function of the Re, $3300 \leq Re \leq 5000$, $m=3$.

Re	3500	3700	3900	3950	3970	4000	4100	4200	4300	4400	4600	5000
δ_Φ	0.009	0.043	0.116	0.112	0.090	0.144	0.158	0.147	0.157	0.144	0.144	0.157

of the various modes in temporally aperiodic regime. Primarily, it concerns the amplitude of modes $m=1$ and $m=4$, but the mode $m=3$ remains dominant when the temporal chaos is progressing.

V. CONCLUSIONS

The thermocapillary flow in cylindrical liquid zone held between two parallel rods at different temperatures is studied under zero-gravity conditions. A parametric investigation of the onset of aperiodicity (chaos) in a liquid bridge is numerically carried out for a medium Prandtl number liquid, $Pr=4$, and unit aspect ratio. The different spatiotemporal patterns of the thermocapillary flow are analyzed, beginning from the onset of instability up to the appearance of the nonperiodic flow and further on (up to $\varepsilon \approx 8.5$). Two-dimensional steady flow becomes oscillatory with azimuthal wave number $m=2$ as the result of a supercritical Hopf bifurcation at $Re_1^{cr}=630$. A second solution with an independent frequency and an independent wave number, $m=3$, is found to appear at $Re_2^{cr} \approx 810$. Two solutions with $m=2$ and $m=3$, each of them being traveling waves with different symmetry patterns, coexist for $Re > Re_2^{cr}$.

The symmetry of the final solution keeps the memory of the initial state of the system for $Re > Re_2^{cr} = 810$; namely, taking an initial guess with $m=1,2,4,6$, etc., symmetries, after some transient time the system will arrive to $m=2$ traveling wave solution. Otherwise, all the odd basic symmetries $m=3,5,7$ (except $m=1$) give $m=3$ traveling wave as final state of the system.

For the $m=2$ solution, the critical mode at the first bifurcation, the flow remains strictly time periodic up to $Re=6000$. Nevertheless, three different regimes have been detected according to the nonlinear characteristics.

The $m=3$ flow pattern manifests another type of the behavior. The motion admits rather strong harmonics in the spectrum just near the onset of the oscillations at $Re_2^{cr} = 810$. It undergoes a transition from the periodic to a weakly chaotic flow via quasi-periodic and period-doubling states. A new frequency ω_1 , relatively small compared to the main one ω_0 , appears in the spectrum at $Re \approx 3300$. The ratio ω_1/ω_0 being larger than 0.5 at the birth of ω_1 is a decreasing function of the Reynolds number, therefore sometimes their ratio becomes irrational. Hence, quasiperiodic regime with two incommensurate frequencies is established. The flow with azimuthal wave number $m=3$ starts exhibiting chaotic

features at $Re \approx 4200$. The onset of temporal nonperiodicity is shown to be associated with development of broadband noise in spectra and preceded by a quasiperiodicity. It can be concluded that the Ruelle-Takens scenario prevails against other ones.

An interesting property of the aperiodic $m=3$ solution is its transition back to a periodic oscillatory behavior at higher values of the Reynolds number. Secondary periodic instability occurs at $Re \approx 5100$. This periodic window spreads at least until $Re=6000$, the largest Reynolds number studied in this paper.

The entropy of the system has been calculated *a posteriori*. The low peak value of the entropy $S=0.09$ for the $m=2$ solutions confirms that a quite ordered flow field oscillates in the liquid bridge. The small changes of the entropy with Re indicate that the energy is spread over a few harmonics. For the $m=3$ flow the peak value $S=0.2$ indicates that the system reveals a weakly chaotic behavior. Inside the region of aperiodicity this maximal value is slightly changed with Re , indicating the numerous dynamic transitions induced by superior harmonics.

The behavior of the net azimuthal flow verifies the existence of the chaotic regime. For the periodic regimes in both cases, $m=2$ and $m=3$, it smoothly grows with the increase of the Reynolds number. But for the quasiperiodic and aperiodic flow states the net azimuthal flow drops down from the regularly growing branch. We can conclude that the energy is transferred from the mean flow into the growing disturbances.

The peak-splitting phenomenon for the $m=3$ flow is inherent to the temperature and the velocity oscillations from the beginning of the quasiperiodic regime. It seems that peak-splitting bifurcation occurs when there is a nonzero phase shift between different harmonics. The experimentally observed in Ref. [8] peak-splitting phenomenon of the temperature oscillations occurs simultaneously with the appearance of the exclusively odd harmonics of ω_0 in the Fourier spectra for $NaNO_3$ liquid zone. In our system we did not notice existence of only even or only odd harmonics.

ACKNOWLEDGMENTS

This work was partially funded by the program on Inter-university Poles of Attraction, initiated by the Belgian State, Prime Minister's Office for Science, Technology and Culture. The authors also gratefully acknowledge discussions with Professor A. Nepomnyashchy of Technion, Israel.

[1] M. Wanschura, V.M. Shevtsova, H.C. Kuhlmann, and H.J. Rath, *Phys. Fluids* **7**, 912 (1995).
 [2] J. Leyboldt, H.C. Kuhlmann, and H.J. Rath, *J. Fluid Mech.* **414**, 285 (2000).
 [3] M. Lappa, R. Savino, and R. Monti, *Int. J. Numer. Methods Fluids* **36**, 53 (2001).
 [4] M.F. Schatz and G.P. Neitzel, *Annu. Rev. Fluid Mech.* **33**, 93 (2001).
 [5] *Growth Mechanism and Dynamics*, edited by D.T.J. Hurle,

Handbook of Crystal Growth (North-Holland, Amsterdam, 1994), Vol. 2.

[6] V. Petrov, A. Haaning, K.A. Muehlner, S.J. Van Hook, and H.L. Swinney, *Phys. Rev. E* **58**, 427 (1998).
 [7] I. Ueno, S. Tanaka, and H. Kawamura, *Phys. Fluids* **15**, 408 (2003).
 [8] S. Frank and D. Schwabe, *Exp. Fluids* **23**, 234 (1997).
 [9] G. L. Baker and J. P. Gollub, *Chaotic Dynamics: An Introduction*, 2nd ed. (Cambridge University Press, Cambridge, 1996).

- [10] V.M. Shevtsova, D.E. Melnikov, and J.C. Legros, *Phys. Fluids* **13**, 2851 (2001).
- [11] V.M. Shevtsova and J.C. Legros, *Phys. Fluids* **10**, 1621 (1998).
- [12] C. A. J. Fletcher, *Computational Techniques for Fluid-Dynamics* (Springer-Verlag, Berlin, 1988).
- [13] V.M. Shevtsova, M. Mojahed, and J.C. Legros, *Acta Astronaut.* **44**, 625 (1999).
- [14] A. Kudrolli and J.P. Gollub, *Physica D* **97**, 133 (1996)
- [15] D. E. Melnikov, V. M. Shevtsova, and J. C. Legros, Proceeding of The World Space Congress, 2002, Houston, IAC-02-0J.4.03, 2002 (unpublished), pp. 1–11.
- [16] S. Wiggins, *Introduction to Applied Nonlinear Dynamical System and Chaos* (Springer, New York, 1990).
- [17] D. Ruelle and F. Takens, *Commun. Math. Phys.* **20**, 167 (1971); *Ann. N.Y. Acad. Sci.* **316**, 408 (1979).
- [18] S. Newhouse, D. Ruelle, and F. Takens, *Commun. Math. Phys.* **64**, 35 (1978).